

## FIRST RESULTS FROM VERY LARGE TELESCOPE NACO APODIZING PHASE PLATE: 4 $\mu\text{m}$ IMAGES OF THE EXOPLANET $\beta$ PICTORIS b\*

SASCHA P. QUANZ<sup>1</sup>, MICHAEL R. MEYER<sup>1</sup>, MATTHEW A. KENWORTHY<sup>2</sup>, JULIEN H. V. GIRARD<sup>3</sup>, MARKUS KASPER<sup>4</sup>, ANNE-MARIE LAGRANGE<sup>5</sup>, DANIEL APAI<sup>6</sup>, ANTHONY BOCCALETTI<sup>7</sup>, MICKAËL BONNEFOY<sup>5</sup>, GAEL CHAUVIN<sup>5</sup>, PHILIP M. HINZ<sup>8</sup>, AND RAINER LENZEN<sup>9</sup>

<sup>1</sup> Institute for Astronomy, ETH Zurich, Wolfgang-Pauli-Strasse 27, 8093 Zurich, Switzerland; [quanz@astro.phys.ethz.ch](mailto:quanz@astro.phys.ethz.ch)

<sup>2</sup> Sterrewacht Leiden, P.O. Box 9513, Niels Bohrweg 2, 2300 RA Leiden, The Netherlands

<sup>3</sup> European Southern Observatory, Alonso de Córdova 3107, Vitacura, Cassilla 19001, Santiago, Chile

<sup>4</sup> European Southern Observatory, Karl Schwarzschild Strasse, 2, 85748 Garching bei München, Germany

<sup>5</sup> Laboratoire d'Astrophysique, Observatoire de Grenoble, Université Joseph Fourier, CNRS, BP 53, F-38041 Grenoble, France

<sup>6</sup> Space Telescope Science Institute, 3700 San Martin Drive, Baltimore, MD 21218, USA

<sup>7</sup> LESIA, UMR 8109 CNRS, Observatoire de Paris, UPMC, Université Paris-Diderot, 5 place J. Janssen, 92195 Meudon, France

<sup>8</sup> Steward Observatory, The University of Arizona, 933 N. Cherry Ave., Tucson, AZ 85721, USA

<sup>9</sup> Max Planck Institute for Astronomy, Königstuhl 17, 69117 Heidelberg, Germany

Received 2010 July 20; accepted 2010 September 2; published 2010 September 17

### ABSTRACT

Direct imaging of exoplanets requires both high contrast and high spatial resolution. Here, we present the first scientific results obtained with the newly commissioned apodizing phase plate coronagraph (APP) on VLT/NACO. We detected the exoplanet  $\beta$  Pictoris b in the narrowband filter centered at 4.05  $\mu\text{m}$  (NB4.05). The position angle ( $209^\circ.13 \pm 2^\circ.12$ ) and the projected separation to its host star ( $0''.354 \pm 0''.012$ , i.e.,  $6.8 \pm 0.2$  AU at a distance of 19.3 pc) are in good agreement with the recently presented data from Lagrange et al. Comparing the observed NB4.05 magnitude of  $11.20 \pm 0.23$  mag to theoretical atmospheric models, we find a best fit with a 7–10  $M_{\text{Jupiter}}$  object for an age of 12 Myr, again in agreement with previous estimates. Combining our results with published  $L'$  photometry, we can compare the planet's [ $L' - \text{NB4.05}$ ] color to that of cool field dwarfs of higher surface gravity suggesting an effective temperature of  $\sim 1700$  K. The best-fit theoretical model predicts an effective temperature of  $\sim 1470$  K, but this difference is not significant given our photometric uncertainties. Our results demonstrate the potential of NACO/APP for future planet searches and provide independent confirmation as well as complementary data for  $\beta$  Pic b.

*Key words:* planets and satellites: detection – planets and satellites: formation – stars: formation – stars: pre-main sequence

*Online-only material:* color figures

### 1. INTRODUCTION

The first images of exoplanets around stars were published in the last two years (HR8799 b, c, d—Marois et al. 2008; Fomalhaut b—Kalas et al. 2008; IRXS J1609-2105—Lafrenière et al. 2008, 2010) following the discovery of a planetary mass companion to the brown dwarf 2MASS1207-3932 in 2005 (Chauvin et al. 2005). For the planets around HR8799, follow-up observations at 3–5  $\mu\text{m}$  revealed evidence for non-equilibrium chemistry in the planetary atmospheres (Janson et al. 2010; Hinz et al. 2010) highlighting the potential of multi-wavelength imagery of extrasolar planetary systems to constrain physical properties in comparison to theoretical atmospheric models.

Lagrange et al. (2009a) detected a planetary mass candidate around the young A-type star  $\beta$  Pictoris (A5V,  $12^{+8}_{-4}$  Myr,  $19.3 \pm 0.2$  pc,  $1.75 M_{\odot}$ ; Zuckerman et al. 2001; Crifo et al. 1997) in  $L'$  images from 2003. After a non-detection based on data obtained in early 2009 (Lagrange et al. 2009b), Lagrange et al. (2010) recently re-detected the planet  $\beta$  Pictoris b which had moved on the other side of the star. The authors constrained the semimajor axis to 8–15 AU (the smallest of all imaged exoplanets today) and derived a mass estimate of  $9 \pm 3 M_{\text{Jupiter}}$ .

Here, using the newly commissioned apodizing phase plate (APP) on VLT/NACO (Kenworthy et al. 2010; Codona et al.

2006), we confirm the detection of  $\beta$  Pictoris b with an independent data set and provide complementary photometry.

### 2. OBSERVATIONS AND DATA REDUCTION

The data were obtained on 2010 April 3, during the commissioning of the APP with the AO high-resolution camera NACO (Lenzen et al. 2003; Rousset et al. 2003) mounted on ESO's UT4 on Paranal. The APP is designed to work in the 3–5  $\mu\text{m}$  range, where it enhances the contrast capabilities between  $\sim 2\text{--}7 \lambda/D$  on one side of the point-spread function (PSF; Kenworthy et al. 2007, 2010). We used the L27 camera ( $\sim 27$  mas pixel<sup>-1</sup>) with the visible wavefront sensor. All images were taken in pupil stabilized mode with the NB4.05 filter ( $\lambda_c = 4.05 \mu\text{m}$ ,  $\Delta\lambda = 0.02 \mu\text{m}$ ).<sup>10</sup> We used the “cube mode” where all data frames are saved individually. To ensure that no frames were lost, we only read out a  $512 \times 512$  pixel sub-array of the detector. As we knew the position angle where the planet was to be expected (Lagrange et al. 2009a, 2009b), we rotated the camera by  $140^\circ$  so that the planet would appear in the “clean,” high-contrast side of the APP PSF (Figure 1, left panel).

We obtained six data cubes of  $\beta$  Pictoris and directly thereafter six data cubes of the PSF reference star HR2435. HR2435 has already been used in previous studies as a reference star for  $\beta$  Pictoris (e.g., Lagrange et al. 2009a), as one can

\* Based on observations collected at the European Organisation for Astronomical Research in the Southern Hemisphere, Chile, under program number 060.A-9800(J).

<sup>10</sup> The APP has been optimized to work with the NB4.05 and IB4.05 filter but it can also be used with the  $L'$  filter (Kenworthy et al. 2010).

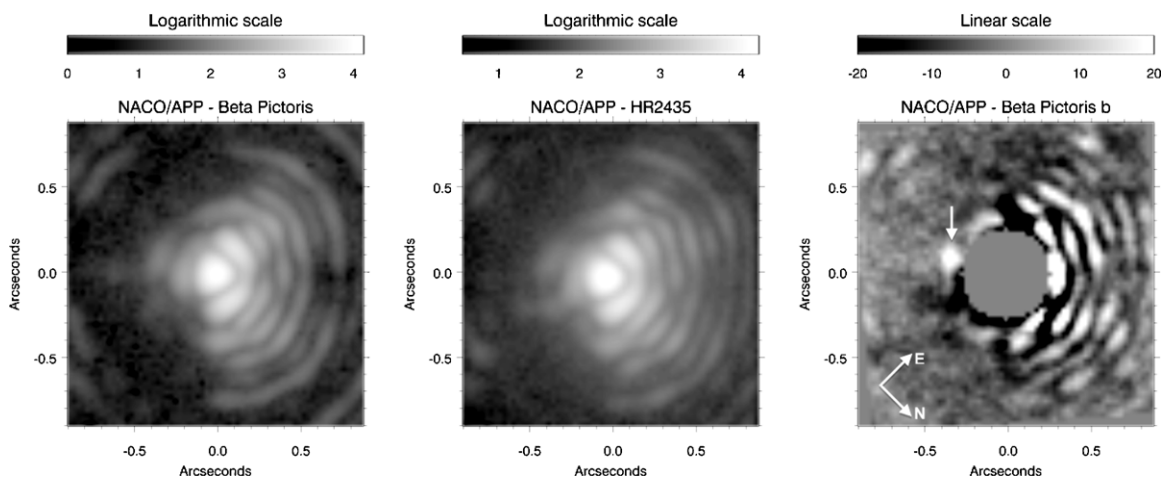


**Figure 1.** Left: median combination of one cube of unsaturated exposures of  $\beta$  Pictoris used to determine the photometry. The effect of the APP can be seen in the left side of the PSF where the diffraction rings are effectively suppressed increasing the contrast between 2 and  $7 \lambda/D$ . Middle: median combination of one cube of saturated exposures of the PSF reference star HR2435. Right: median combination of all PSF-subtracted science exposures.  $\beta$  Pictoris b is indicated by the arrow. The right side suffers from subtraction residuals as does the central region of the PSF, which has been masked out.

**Table 1**  
Summary of Observations on 2010 April 3

Parameter	$\beta$ Pictoris	HR2435
UT start	00:39:31.1	01:34:21.3
NDIT $\times$ DIT <sup>a</sup>	200 $\times$ 1 s	200 $\times$ 1 s
NINT <sup>b</sup>	6	6
Parallactic angle start	69:469	69:451
Parallactic angle end	74:492	74:499
Air mass	1.38–1.44	1.42–1.48
Typical DIMM seeing (EC) <sup>c</sup>	0'.70–0'.90	0'.60–0'.75
$\langle\tau_0\rangle$ <sup>d</sup>	4.3–7.9 ms	4.0–7.8 ms

#### Notes.

<sup>a</sup> NDIT: the number of detector integration times (i.e., number of individual frames); DIT: detector integration time (i.e., single frame exposure time).

<sup>b</sup> NINT: the number of integrations or data cubes ( $2 \times 3$  dither positions = 6 data cubes).

<sup>c</sup> Average value of the coherent energy of the PSF per data cube. Calculated by the Real Time Computer of the AO system.

<sup>d</sup> Average value of the coherence time of the atmosphere per data cube. Calculated by the Real Time Computer of the AO system.

obtain data at matching parallactic angles. Also, the star is close in the sky and has a similar brightness providing comparable AO correction. For both sources, each data cube was taken at a slightly different dither position following a three-point dither pattern which was repeated twice. The on-source integration time was 20 minutes each. Table 1 summarizes the observations and the observing conditions. We chose to saturate the core of the stellar PSFs, but we note that the APP reduces the peak flux in the PSF core by roughly 40% so that the comparatively long exposure time of 1 s did not lead to saturation effects outside of the inner  $\sim 5$  pixels.

For the photometric calibration, we also obtained unsaturated images of  $\beta$  Pictoris ( $\sim 50\%$  Full Well) prior to the science observations described above. We used the same observing strategy but decreased the detector integration time to 0.2 s.

The data reduction was done using self-developed IDL routines. The following steps were applied to all three data sets (i.e.,  $\beta$  Pictoris unsaturated and saturated images, HR2435 saturated images). First, in order to eliminate the sky background

emission, we subtracted from each individual frame the corresponding frame from another cube taken at a different dither position (e.g., Cube 2 frame 10–Cube 3 frame 10) and vice versa. As the first two frames in each cube always showed a higher detector noise level they were disregarded. We also disregarded frames where the AO correction was poor (flux measured in the PSF core less than 50% compared to the previous frame). Then, bad pixels and cosmic ray hits deviating by more than  $3\sigma$  in a  $5 \times 5$  pixel box were replaced with the mean of the surrounding pixels. After this we continued as follows: the unsaturated  $\beta$  Pictoris images were aligned and cube-wise median combined, yielding six final images on which we performed photometry (Figure 1, left panel). The alignment of the images was done using cross-correlation where the optimal shift between two images was determined with an accuracy of 0.1 pixel. The same procedure was applied to the saturated HR2435 images yielding six individual reference PSF images (i.e., one per cube; Figure 1, middle panel). The individual frames were not dithered to the same field orientation before the combination, so that all static telescope aberrations remained constant throughout the cubes and in the final images. For the saturated frames of  $\beta$  Pictoris, we determined the parallactic angle for each individual frame by linear interpolation between the first frame and the final frame in each cube.<sup>11</sup> Using cross-correlation, all frames from all cubes were then aligned to the same reference image for which we used the final, median-combined image of the first cube of the unsaturated  $\beta$  Pictoris exposures. Thereafter we aligned, scaled, and subtracted one of the six final HR2435 reference PSFs from each individual saturated  $\beta$  Pictoris frame. The choice of the reference PSF was a trade-off between matching parallactic angle and observing conditions in the individual cubes. The best results (i.e., strongest signal of the planet, least residuals) were obtained using reference PSF 2 for the frames in cubes one and two, PSF 3 for cubes three and four, and PSF 5 for cubes five and six. The scaling was done in the bright, right-hand side of the PSF where the diffraction rings were clearly visible. We scaled the reference PSF by minimizing the mean in the subtracted images in a semi-annulus centered on the star with an inner radius of 15 pixels, an outer radius of 27 pixels

<sup>11</sup> Per default, only the parallactic angle at the beginning and at the end of each cube are saved in the fits header in NACO's cube mode.

(i.e., covering the 3rd and 4th Airy ring), and an opening angle of  $150^\circ$ . Finally, we de-rotated all PSF-subtracted frames to match the parallactic angle of the first frame and created a median combined final image.

### 3. RESULTS

#### 3.1. The Detection of $\beta$ Pic b

The right-hand panel in Figure 1 shows the final image of the data reduction process. The exoplanet is clearly detected in the left side of the image. We conducted several tests to exclude the possibility of a false detection. (1) We created final images for each individual cube by derotating and combining the respective PSF-subtracted images. The planet was detected in the final images of all six cubes. (2) Comparing the position angle of the exoplanet in the final images of the individual cubes revealed the expected rotation introduced by the pupil tracking mode. (3) Speckles can appear along the spider arms holding the secondary mirror of the telescope, but the nearest arm of the telescope spider was  $\gtrsim 20^\circ$  away from the position of the planet. Also, (4) we implemented a second independent data reduction pipeline based on the LOCI algorithm (Lafrenière et al. 2007). As the small-field rotation in our data set did not allow us to construct a reference PSF directly from the  $\beta$  Pic images (Angular Differential Imaging; e.g., Marois et al. 2006), we used the HR2435 data set. For each  $\beta$  Pic frame, we constructed a reference PSF based on a linear combination of the final HR2435 images so that the residuals in the high-contrast side of the PSF were minimized. With this approach, we also recovered the signal of the exoplanet at the same position.

The projected separation between star and planet is  $0''.354 \pm 0''.012$  (i.e.,  $6.8 \pm 0.2$  AU at a distance of 19.3 pc) and the position angle is  $209^\circ 13' \pm 2'' 12'$  (east of north). The values are mean values derived from the six final PSF-subtracted cube images (see, test (2) above) and the errors include the corresponding standard deviation of the mean and systematic uncertainties from the alignment of the images. The position of the star in the unsaturated reference image used for the alignment and the position of the planet in the six final images were determined by fitting a two-dimensional Gaussian to the respective source. For our final astrometric numbers, we had to rely on the plate scale and field orientation provided in the header of the images as we did not observe an astrometric calibrator. However, potential deviations are expected to be small compared to our errors (Lagrange et al. 2009a). Comparing the final numbers to the results from Lagrange et al. (2010), we find that the position angle is in very good agreement and the separation appears to have increased as expected from the planet's orbital motion. However, the short time baseline between our data and the data from Lagrange et al. (2010) does not allow us to put any new constraints on the planet's actual orbit.

#### 3.2. Photometry and Color of $\beta$ Pic b

To derive the relative photometry between the planet and its star, we used an aperture with a radius of 2 pixels and computed the mean flux of  $\beta$  Pictoris in the six final unsaturated images and the mean flux of the planet in the six final PSF-subtracted cube images. The flux derived from the unsaturated images was scaled to account for the difference in the integration time. Each flux measurement was corrected for residual background emission by measuring and subtracting the mean flux per pixel in a semi-annulus centered on the planet as well as on the star. The semi-annulus covered only the high-contrast side of the

objects and had an inner and outer radius of 5 and 8 pixels for the planet and of 18 and 25 pixels for the star. The contrast between the star and the planet in the NB4.05 filter amounts to  $\Delta m_{4.05} = 7.75 \pm 0.23$  mag. The error was derived from error propagation taking into account the standard deviations of the mean of both the flux of the planet and the flux of the unsaturated  $\beta$  Pictoris images.

In the  $L'$  filter, the contrast between the planet and the star is  $\Delta m_{L'} = 7.7 \pm 0.3$  mag<sup>12</sup> which, combined with the stars apparent magnitude of  $L' = 3.454 \pm 0.003$  mag (Bouchet et al. 1991), translates into an apparent magnitude for the exoplanet of  $m_{L'} = 11.15 \pm 0.3$  mag. Since an A5V star has an  $[L' - M]$  color of  $\sim 0.01$  mag, we can assume that the intrinsic  $[L' - \text{NB4.05}]$  color of  $\beta$  Pic is negligible. Based on the observed contrast in the NB4.05 filter, the exoplanet's apparent magnitude is then  $m_{\text{NB4.05}} = 11.20 \pm 0.23$  and its color  $[L' - \text{NB4.05}] = -0.05 \pm 0.38$  mag.

#### 3.3. Color Comparison to Cool Field Dwarfs

Cushing et al. (2008) published NIR spectra for cool L and T field dwarfs that cover the NB4.05 filter but terminate before the long wavelengths cutoff of ESO's  $L'$  filter. However, for some of these objects Leggett et al. (2002) published  $L'$  photometry. To obtain the magnitudes in the NB4.05 filter, we used the filter transmission curve and convolved it with the spectra from Cushing et al. (2008). The zero point of the filter was derived from a Kurucz model of an A0V star. Using the  $L'$  filter transmission curve, we first scaled the Kurucz model to the observed flux density of Vega in the  $L'$  filter. For this, we assumed  $m_{L'}^{\text{Vega}} = m_V^{\text{Vega}} = 0.03$  mag and  $F_V^{\text{Vega}} = 246.105$  Jy or  $F_\lambda^{\text{Vega}} = 5.219 \cdot 10^{-11} \text{ W m}^{-2} \mu\text{m}^{-1}$  in the ESO  $L'$  filter. Then, we measured the flux density of the A0V star in the NB4.05 filter and derived the zero point assuming the star has the same magnitude here. The derived flux densities of the field objects could then be converted into magnitudes, and we determined the  $[L' - \text{NB4.05}]$  color for the objects. The error in the magnitude in the NB4.05 filter was derived from computing a minimum and a maximum magnitude by either subtracting or adding the mean error of the spectra in that wavelength range. Whatever resulted in a bigger deviation from the mean magnitude was used as (conservative) error bar. Finally, as the  $L'$  photometry from Leggett et al. (2002) was done in the MKO photometric system and not in the ESO system, we applied a first order correction by subtracting the zero point offset of 0.02 mag<sup>13</sup> from the quoted photometric measurements.

In Figure 2, we plot the spectral type of the field objects against their color (black points). Data were available for spectral types L1, L3.5, L7.5, T2, and T5.<sup>14</sup> Fitting a straight line to the data points, we find that the color of  $\beta$  Pic b is most similar to that of a field object with a spectral type of L4. However, spectral types from L0 to L7 are consistent with the observed color given the large error bars. For field objects around spectral type L4, Cushing et al. (2008) found effective temperatures of 1700 K which is the same temperature one obtains using the spectral type–temperature relation derived by Golimowski et al. (2004). We note, however, that the surface

<sup>12</sup> This figure was obtained from the 2009 October data set in Lagrange et al. (2010) as well as from the 2003 November data set in Lagrange et al. (2009a).

<sup>13</sup> See <http://www.gemini.edu/sciops/instruments/midir-resources/imaging-calibrations/fluxmagnitude-conversion>

<sup>14</sup> Optical spectral types differ slightly from NIR spectral types for three sources. However, the outcome of this analysis remains unchanged if we use the NIR spectral types instead.



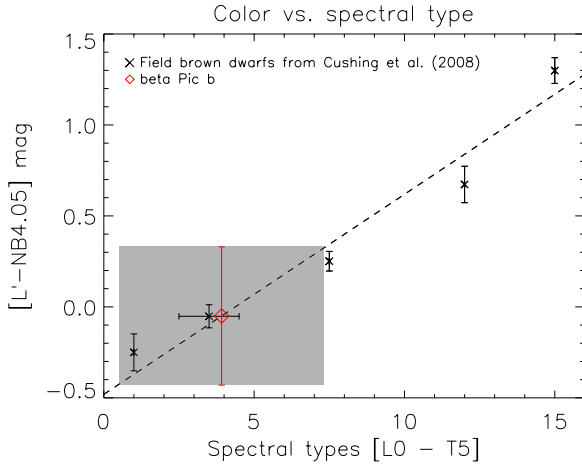


**Figure 2.**  $[L' - \text{NB4.05}]$  color as function of spectral type derived from cool field dwarf (black points). The dashed line is a linear fit to the field dwarf data. The position of  $\beta$  Pic b on the fitted correlation is shown in red. The error bars are the root sum squares of the photometric errors in the individual filters. The shaded area covers the range of spectral types consistent with the color of the exoplanet given the error bars.

(A color version of this figure is available in the online journal.)

gravity of the young exoplanet is expected to be much lower than that of the field objects ( $\log g \approx 4.0$  rather than 4.5–5.5 for field L/T dwarfs; Cushing et al. 2008).

### 3.4. Comparison to Atmospheric/Evolutionary Models

In Figure 3, we compare the observed magnitudes to theoretical isochrones for low-mass objects based on the DUSTY models from Chabrier et al. (2000). These evolutionary models are based on a spherical collapse model where the objects start initially with very large radii and their internal energy is dominated by contraction. Using a distance of 19.3 pc and assuming an age of 12 Myr, we find a mass of 7–10  $M_{\text{Jupiter}}$  which agrees with the 6–12  $M_{\text{Jupiter}}$  derived from the  $L'$  filter. Here, the mass range is only determined by the photometric uncertainties. The most likely mass based on the NB4.05 magnitude is 8  $M_{\text{Jupiter}}$  which corresponds to  $T_{\text{eff}} \approx 1470$  K and  $\log g \approx 4.0$ . Assuming an age of 20 Myr, this mass would increase to 11  $M_{\text{Jupiter}}$  with  $T_{\text{eff}} \approx 1425$  K and  $\log g \approx 4.1$ , while for 8 Myr we would estimate 6  $M_{\text{Jupiter}}$  with  $T_{\text{eff}} \approx 1380$  K and  $\log g \approx 3.9$ .

### 3.5. Contrast Curve Analysis

Using the final image (right panel, Figure 1), we computed a contrast curve showing the detection limit for potential additional companions as a function of radius (Figure 4). To derive the curve, we computed the standard deviation  $\sigma$  of the pixel values in semi-annuli (5 pixel width) as a function of radial distance from the center in the high-contrast side of the image. The signal and the noise of a hypothetical companion can be written as

$$S = n \cdot \eta \cdot \sigma \quad (1)$$

and

$$N \approx \sqrt{n} \cdot \sigma, \quad (2)$$

with  $n$  being the number of pixels in the chosen photometric aperture (here  $n = \pi \cdot 2^2 \approx 12.56$ ) and  $\eta$  being a factor that depends on the chosen signal-to-noise ratio (S/N) one wants to achieve. For an S/N of 5,  $\eta$  can be derived from

$$\frac{S}{N} = 5 \approx \sqrt{n} \cdot \eta. \quad (3)$$

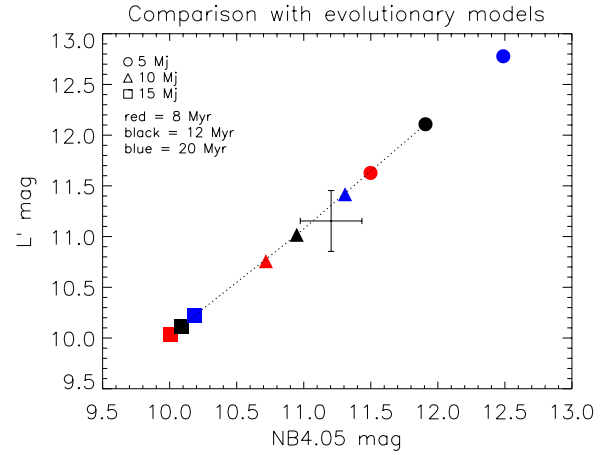


**Figure 3.** Apparent  $L'$  and NB4.05 magnitudes of  $\beta$  Pic b (black cross) compared to theoretical isochrones based on the DUSTY models from Chabrier et al. (2000). Circles, triangles, and boxes denote objects with 5, 10, and 15  $M_{\text{Jupiter}}$ , respectively. The age of the objects is color-coded with red symbols being 8 Myr, black being 12 Myr, and blue being 20 Myr. The dashed black line shows the 12 Myr isochrone.

(A color version of this figure is available in the online journal.)

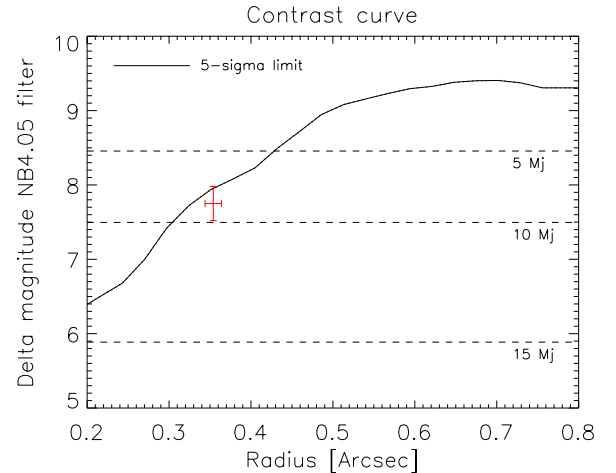


**Figure 4.**  $5\sigma$  contrast curve derived from the high-contrast side in final PSF-subtracted image shown in the right panel of Figure 1. The dashed horizontal lines correspond to masses as predicted by the DUSTY models (Chabrier et al. 2000) for an assumed age of 12 Myr. The red cross shows the position of  $\beta$  Pic b.

(A color version of this figure is available in the online journal.)

The ratio between the signal of a planet with an S/N of 5 (Equation (1)) and the mean flux of beta Pictoris computed in a 2 pixel aperture relates to a difference in magnitude which we compute as a function of  $\sigma(r)$  (Figure 4). As the noise of the residuals is not perfectly Gaussian in all annuli (see also, e.g., Kasper et al. 2007), we chose to plot the conservative  $5\sigma$  limit only. A more sophisticated analysis, i.e., the insertion of fake planets, may result in a somewhat different contrast curve.

## 4. DISCUSSION

$\beta$  Pictoris b is an exoplanet whose estimated mass, age, and separation are in agreement with predictions from core accretion planetary formation models (see, Lagrange et al. 2010, and references therein). It is interesting to note that dynamical studies analyzing the sub-structure of the remnant debris disk around  $\beta$  Pic predicted the mass and the orbit of

the planetary companion before it was imaged (e.g., Mouillet et al. 1997; Augereau et al. 2001). It was shown that an object with a mass significantly higher than  $\sim 10 M_{\text{Jupiter}}$  would create much larger disk asymmetries. Thus, the dynamical analysis provides further support for the mass estimates derived from the observed photometry and the evolutionary models. This in turn led Lagrange et al. (2010) to the conclusion that the “cold start” evolutionary models of young, giant planets (Fortney et al. 2008) are not in agreement with  $\beta$  Pic b. These models predict the planet to be significantly less luminous for its age and dynamically predicted mass. Our new flux point at 4.05  $\mu\text{m}$  confirms the brightness of the source and supports the argument from Lagrange et al. (2010). However, given the comparatively large uncertainties in the observed fluxes, we refrain from undertaking a more comprehensive comparison to additional sets of evolutionary and atmospheric models (e.g., Burrows et al. 2006). For instance for an assumed age of 12 Myr the models from Chabrier et al. (2000) predict  $[L' - \text{NB4.05}] \leq 0.3$  mag for all objects between 4 and 100  $M_{\text{Jupiter}}$ . Also, the apparent difference in effective temperature of  $\beta$  Pic b derived in Sections 3.3 and 3.4 is not statistically significant. Given the error bars in Figure 2,  $T_{\text{eff}}$  as high as  $\sim 1700$  K is still consistent with the observed magnitudes within  $2\sigma$ .

Future observations at different wavelengths will help us to better constrain the atmospheric parameters and composition of  $\beta$  Pic b and to check whether the preliminary result, that the models predict a lower  $T_{\text{eff}}$  than the comparison to field dwarfs, persists. A frequent monitoring of the exoplanet’s position will eventually allow us to determine the orbital parameters with higher accuracy.

This research has made use of the SIMBAD database, operated at CDS, Strasbourg, France. We are indebted to Michael Cushing, Isabelle Baraffe, Udo Wehmeier, and the ESO staff on Paranal, in particular Jared O’Neal, for their support. We also thank the referee for useful comments and suggestions.

*Facilities:* VLT:Yepun (NACO)

## REFERENCES

- Augereau, J. C., Nelson, R. P., Lagrange, A. M., Papaloizou, J. C. B., & Mouillet, D. 2001, *A&A*, **370**, 447
- Bouchet, P., Schmider, F. X., & Manfroid, J. 1991, *A&AS*, **91**, 409
- Burrows, A., Sudarsky, D., & Hubeny, I. 2006, *ApJ*, **640**, 1063
- Chabrier, G., Baraffe, I., Allard, F., & Hauschildt, P. 2000, *ApJ*, **542**, 464
- Chauvin, G., Lagrange, A., Dumas, C., Zuckerman, B., Mouillet, D., Song, I., Beuzit, J., & Lowrance, P. 2005, *A&A*, **438**, L25
- Codona, J. L., Kenworthy, M. A., Hinz, P. M., Angel, J. R. P., & Woolf, N. J. 2006, *Proc. SPIE*, **6269**, 62691N
- Crifo, F., Vidal-Madjar, A., Lallement, R., Ferlet, R., & Gerbaldi, M. 1997, *A&A*, **320**, L29
- Cushing, M. C., et al. 2008, *ApJ*, **678**, 1372
- Fortney, J. J., Marley, M. S., Saumon, D., & Lodders, K. 2008, *ApJ*, **683**, 1104
- Golimowski, D. A., et al. 2004, *AJ*, **127**, 3516
- Hinz, P. M., Rodigas, T. J., Kenworthy, M. A., Sivanandam, S., Heinze, A. N., Mamajek, E. E., & Meyer, M. R. 2010, *ApJ*, **716**, 417
- Janson, M., Bergfors, C., Goto, M., Brandner, W., & Lafrenière, D. 2010, *ApJ*, **710**, L35
- Kalas, P., et al. 2008, *Science*, **322**, 1345
- Kasper, M., Apai, D., Janson, M., & Brandner, W. 2007, *A&A*, **472**, 321
- Kenworthy, M. A., Codona, J. L., Hinz, P. M., Angel, J. R. P., Heinze, A., & Sivanandam, S. 2007, *ApJ*, **660**, 762
- Kenworthy, M. A., Quanz, S. P., Meyer, M. R., Kasper, M. E., Lenzen, R., Codona, J. L., Girard, J. H. V., & Hinz, P. M. 2010, arXiv:1007.3448
- Lafrenière, D., Jayawardhana, R., & van Kerkwijk, M. H. 2008, *ApJ*, **689**, L153
- Lafrenière, D., Jayawardhana, R., & van Kerkwijk, M. H. 2010, *ApJ*, **719**, 497
- Lafrenière, D., Marois, C., Doyon, R., Nadeau, D., & Artigau, É. 2007, *ApJ*, **660**, 770
- Lagrange, A., et al. 2009a, *A&A*, **493**, L21
- Lagrange, A., et al. 2009b, *A&A*, **506**, 927
- Lagrange, A.-M., et al. 2010, *Science*, **329**, 57
- Leggett, S. K., et al. 2002, *ApJ*, **564**, 452
- Lenzen, R., et al. 2003, *Proc. SPIE*, **4841**, 944
- Marois, C., Lafrenière, D., Doyon, R., Macintosh, B., & Nadeau, D. 2006, *ApJ*, **641**, 556
- Marois, C., Macintosh, B., Barman, T., Zuckerman, B., Song, I., Patience, J., Lafrenière, D., & Doyon, R. 2008, *Science*, **322**, 1348
- Mouillet, D., Larwood, J. D., Papaloizou, J. C. B., & Lagrange, A. M. 1997, *MNRAS*, **292**, 896
- Rousset, G., et al. 2003, *Proc. SPIE*, **4839**, 140
- Zuckerman, B., Song, I., Bessell, M. S., & Webb, R. A. 2001, *ApJ*, **562**, L87